nature geoscience

SUPPLEMENTARY INFORMATION

DOI: 10.1038/NGEO1169

Chinese stalagmite δ^{18}O controlled by changes in the Indian monsoon during a simulated Heinrich event Supplementary Information

Francesco S. R. Pausata[1,2*], David S. Battisti[3,2], Kerim H. Nisancioglu[1,4] and Cecilia M. Bitz[3]

[1]Bjerknes Center for Climate Research, Bergen, Norway

[2]Geophysical Institute, University of Bergen, Bergen, Norway

[3]Department of Atmospheric Sciences, University of Washington, Seattle (WA), USA

[4]UNI Research, Bergen, Norway

[*]now at the Joint Research Center, Institute for Environment and Sustainability, Ispra (VA), Italy

Comparison of the difference in the H1 and LGM climates simulated by CAM3 and CCSM3

The objective of our study is to examine the response of the climate system, including the isotopic composition of precipitation, to a sudden injection of freshwater in the North Atlantic associated with a Heinrich-like event. Such *climate* experiments have been performed with a handful of climate models, including the NCAR Community Climate System Model, version 3 (CCSM3) (*1,2*). Hence, we took as the starting point for our study the climate of the Last Glacial Maximum (LGM) as simulated by the CCSM3 when forced by insolation, carbon dioxide, ice sheets and continental geometry from 21 kyrs BP. The simulated LGM climate has been described in Otto-Bleisner et al 2006 (*3*), among others; the boundary conditions and forcing for the LGM simulation follow the protocol established by PMIP2 (*4*). The same coupled model has also previously been used to examine the climate response associated with a sudden increase in freshwater associated with a typical Heinrich event during the LGM (*1,2*). Bitz et al (*1*) added 16 Sv yr of water to the North Atlantic and Arctic Ocean at three unique points in time in the aforementioned LGM simulation to examine the response of the climate to a Heinrich event (see Hemming (*5*) for an excellent discussion of the freshwater discharge associated with a typical Heinrich event). The freshwater experiments were then averaged to create the ensemble averaged coupled model response to the freshwater dump, which we call the coupled model H1 response.

The coupled model used in the aforementioned experiments did not contain a module for isotopes of water. Rather than re-do these expensive and time-consuming coupled experiments, we performed offline experiments using the identical atmosphere model that was in the LGM and H1 coupled CCSM3 experiments but it has embedded in it a module for water isotopes. The atmosphere model is the Community Atmosphere Model version 3, CAM3, (*6*). In both

the coupled and uncoupled experiments, the model is deployed with a spatial resolution that is roughly 2.8° by 2.8° (T42) and it has 26 vertical levels. The water isotope module has been provided by David Noone. In general, the isotopic composition of precipitation in CAM3 for the present day climate is reproduced by the model (*7*).

The uncoupled atmosphere model is forced with the same insolation, ice sheets and carbon dioxide as in the LGM and H1 coupled model experiments, as well as with the SST that was simulated in the coupled LGM and H1 experiments. This off-line methodology for simulating the isotopic response to a Heinrich event is appropriate if the climate from the uncoupled experiments is very close to that from the coupled experiments, which is indeed the case. For brevity, we show only the change in the temperature and precipitation due to the freshwater dump (H1 minus LGM) that results from using the coupled model and the uncoupled model. The atmospheric circulation and the spatial and seasonal changes in surface temperature and precipitation in the uncoupled experiments are very similar to those from the coupled experiments (cf. Fig. 1 and Fig. S1), which allows us to use the uncoupled LGM and H1 experiments to determine changes in the precipitation weighted isotopes associated with abrupt changes in sea ice in the North Atlantic.

It is interesting to note that extension of the sea ice associated with the freshwater dump into the North Atlantic causes an annual averaged cooling everywhere in the Northern Hemisphere except over central India and eastern Tibet, where it actually warms. The warming in central India is due to change in the surface energy budget in summertime associated with the weakened monsoon. The warming in northern India and northeast TIbet is a wintertime phenomenon (not shown) that is due to an anomalous southerly low level wind (between the surface and about 500hPa) in H1 experiment compared to the LGM experiment, which causes anomalous warm air advection into northern India. These wind anomalies are part of a low (high) level anomalous anticyclone (cyclone) that is forced by the reduced wintertime precipitation just north of the

equator to the southeast of India (not shown) associated with colder ocean (see the top two panels in Fig S8). The structure, location and spatial scale of these wind anomalies are very similar to the canonical response of the tropical atmosphere to asymmetric SST anomalies deep in the tropics (*8*).

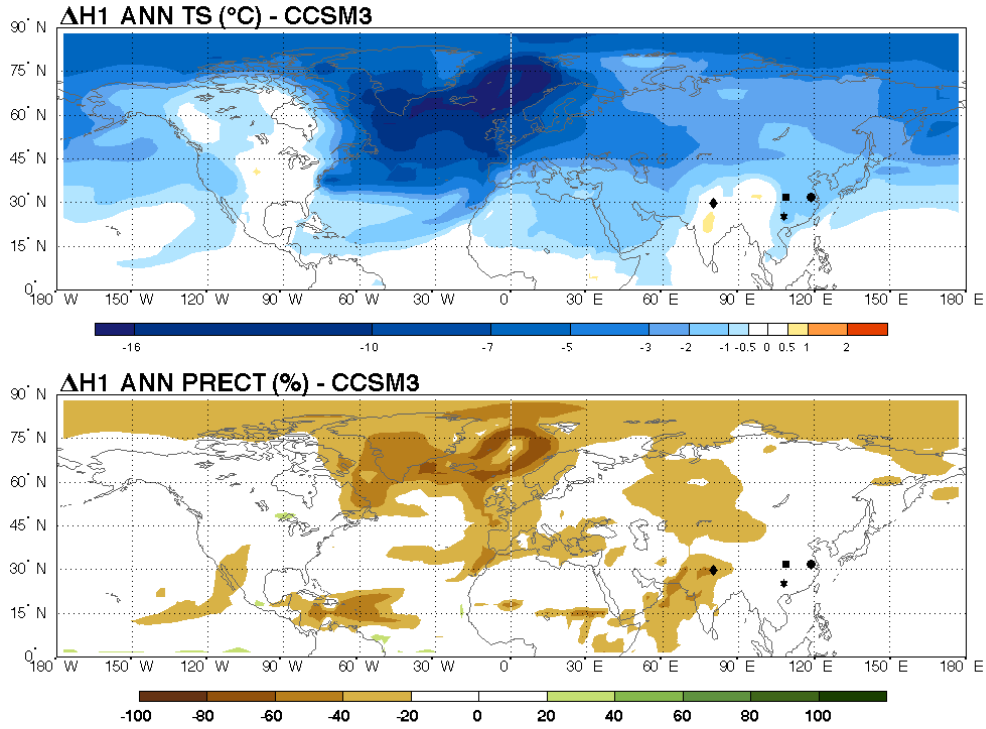

Fig. S1: Change in the annual averaged (top) surface temperature and (bottom) precipitation (in %) in CCSM3 due to the Heinrich event, "H1 minus LGM". Markers indicate the location of the following caves: Hulu (circle), Songjia (square), Dongge (star), Timta (diamond).

Precipitation weighted δ^{18}O

At each location, the δ^{18}O values shown in this study are weighted by the amount of precipitation:

$$\delta^{18}O^{WGT} = \frac{\sum_k \sum_j (\delta^{18}O_{j,k} * PRECT_{j,k})}{\sum_k \sum_j PRECT_{j,k}} ..., \quad (1)$$

where j is the index referring to the time series we are considering (annual, monthly, etc.), δ^{18}O is the isotopic composition of the precipitation, and $PRECT$ is the net monthly precipitation. When considering the climatological average precipitation weighted δ^{18}O ($\equiv \delta^{18}O_p$), the double sum is done over $j = 1, 2...11, 12$ months and $k = 1, 2, ..., 14, 15$ years of monthly values, which is sufficient to ensure the changes discussed in this work are statistically significant.

The contribution of summer time changes to the changes in $\delta^{18}O_p$

Here we show that most of the change in $\delta^{18}O_p$ is due to summertime changes in the δ^{18}O of precipitation. We consider summer the period of the East Asian summer monsoon (EASM) that goes from May to August (MJJA), because that is when most of the precipitation occurs at the Chinese caves. The left panel in Fig. S2 shows the total change in $\delta^{18}O_p$ in the H1 experiment compared to the LGM experiment (H1 minus LGM). The right panel of Fig. S2 shows the change in $\delta^{18}O_p$ when only changes in summer (MJJA) precipitation and in the summer δ^{18}O of precipitation from the H1 experiment are included in the calculation of $\delta^{18}O_p$ (the LGM precipitation and δ^{18}O of precipitation are retained in the non-summer months). The similarity in the amplitude and patterns of the $\delta^{18}O_p$ changes in these two panels attests to the importance of summertime changes.

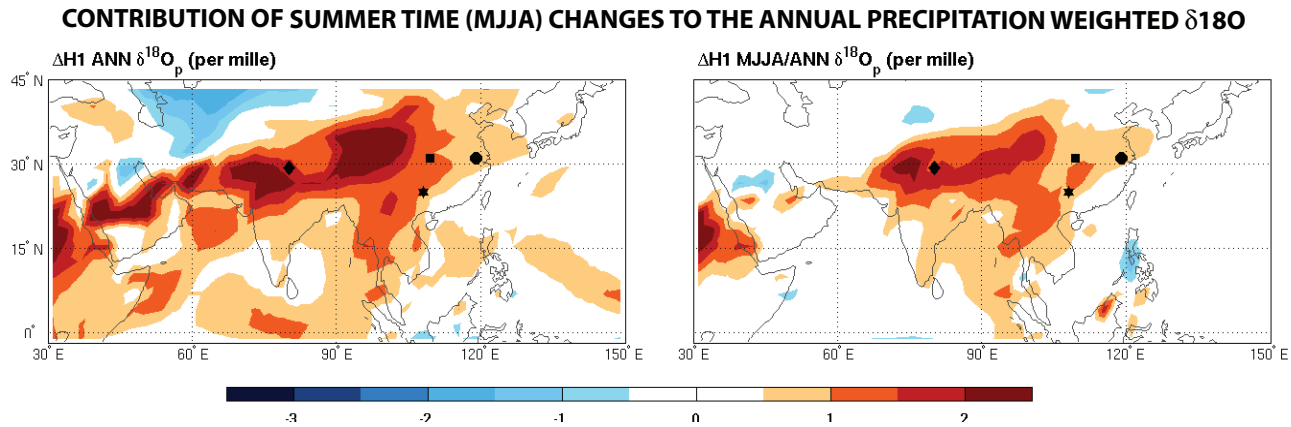

Fig. S2: H1 minus LGM difference of precipitation weighted $\delta^{18}O_p$ (left) and the summertime (MJJA) contribution to $\delta^{18}O_p$ (right). Markers indicate the location of the following caves: Hulu (circle), Songjia (square), Dongge (star), Timta (diamond).

The contribution of changes in the precipitation and δ^{18}O to the net change in $\delta^{18}O_p$

Even without changes to the isotopic composition of precipitation, changes in the amount of precipitation in summertime would cause changes in $\delta^{18}O_p$ because the isotopic composition of summer precipitation is much lighter than winter precipitation; this is the so-called "seasonality effect". Since there is little change in summertime precipitation over China in the H1 experiment, we do not anticipate that changes in seasonality can account for the change in $\delta^{18}O_p$ in the Chinese caves. This is confirmed in Fig. S3, where we show the *monthly* weighted δ^{18}O of precipitation from the LGM and H1 experiments (solid red and blue curves respectively) as well as the *monthly* weighted δ^{18}O of precipitation for the LGM and H1 experiments when the precipitation amount is replaced by that from the H1 and LGM experiments respectively (the red and blue dashed lines, respectively)[1]. The difference between the solid and dashed lines is

[1]The *monthly* weighted δ^{18}O of precipitation is defined in Eq. 1 where the sum is done only over $k = 1, 15$ years for a single month. For example, the monthly weighted δ^{18}O of precipitation for January includes the sum over all Januaries ($j = 1, k = 1, ...15$).

an indication of the importance of changes in the amount of precipitation. For the three Chinese caves, the change in monthly δ^{18}O between the H1 and LGM is overwhelmingly due to changes in the δ^{18}O of the incoming vapor; changes in the seasonality are inconsequential for explaining the net change in $\delta^{18}O_p$. For the Indian cave, however, changes in both the seasonality and the isotopic composition of precipitation contribute remarkably to the simulated change in $\delta^{18}O_p$.

Origin of the water that falls at the cave sites in the LGM and H1 experiments

Water vapor from selected regions was tagged in order to distinguish the main moisture sources for each cave and ascertain which water mass is affecting the δ^{18}O recorded by the speleothems. We selected ten different regions: North and South Pacific Ocean; the North-East, South-East, North-West and South-West Tropical Pacific; Arabian Sea; Gulf of Bengal; continental regions; and everywhere else (Fig. S4). For simplicity, we show the result for four regions: the whole Tropical Pacific, the whole Indian Ocean, the continental regions, and everywhere else. We followed the vapor until it precipitated and then we recorded at each point the δ^{18}O of precipitation and the amount of precipitation from each given region. Hence, for every point on the globe and every point in time, we have a record of the amount and isotopic composition of the precipitation that originates in each of the four regions.

For each cave site, figure S5 shows the fraction of the total precipitation that falls during the monsoon season (MJJA) that originates from the Indian Ocean, the Pacific Ocean and the continents (the residual includes the precipitation from all other areas). At each cave site, the relative contribution of each region to the total precipitation in the H1 experiment is very similar to that in the LGM experiment – so much so that their contribution to the net change in simulated $\delta^{18}O_p$ is less than 10 percent.

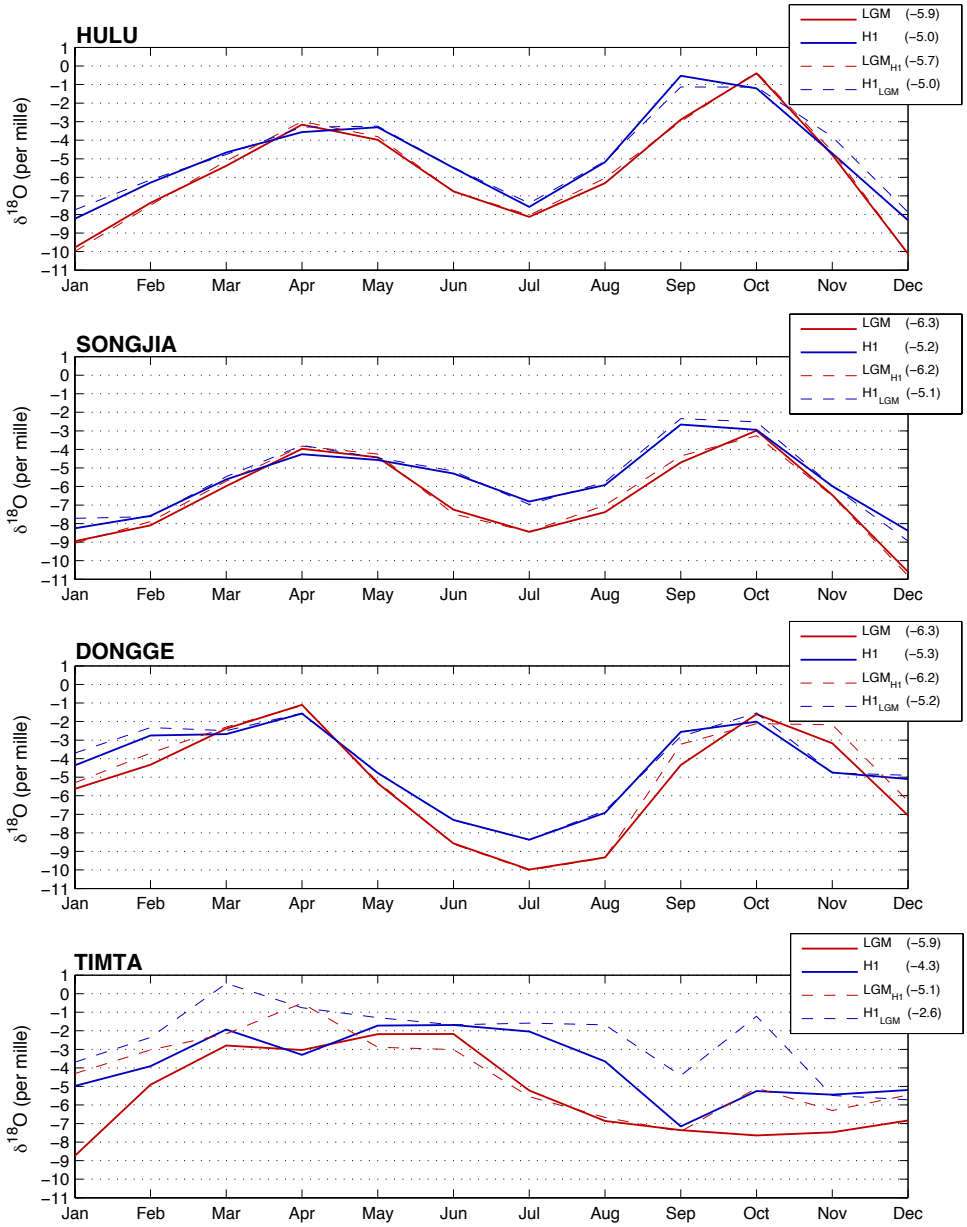

Fig. S3: Monthly precipitation weighted δ^{18}O for the LGM (red solid) and H1 (blue solid) experiments at each of the cave sites shown in Fig. S1. The dashed lines show the monthly δ^{18}O in the LGM weighted by the precipitation from the H1 experiment (red dashed) and the monthly δ^{18}O in the H1 weighted by the precipitation from the LGM experiment (blue dashed). In brackets is the precipitation weighted $\delta^{18}O_p$ for each combination.

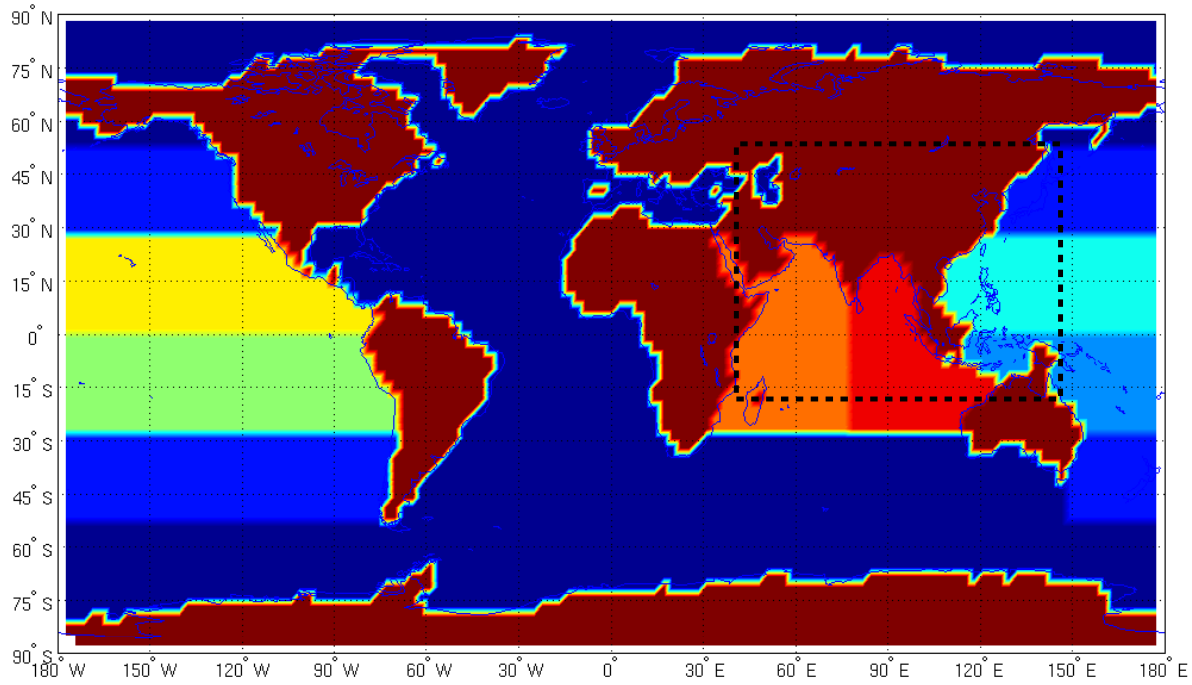

Fig. S4: Tagged regions used to ascertain the source of water vapor at the cave sites. The stippled box marks the area shown in Fig. S9.

Relationship between the change in SST and the change in temperature and precipitation

In order to understand the linkages between the changes in climate and the changes in the isotopic composition of precipitation, we performed three additional experiments with the atmosphere model. Starting from the prescribed boundary conditions from the LGM experiment, we made regional modifications to the SST and sea ice extent to be identical to that in the H1 experiment. These experiments were designed to isolate the impact of the SST and sea ice changes in a specific ocean basin on the temperature and precipitation, on the isotopic composition of precipitation, and on the origin of the vapor that is eventually precipitated over southern and eastern Asia. The sensitivity experiments we have performed are:

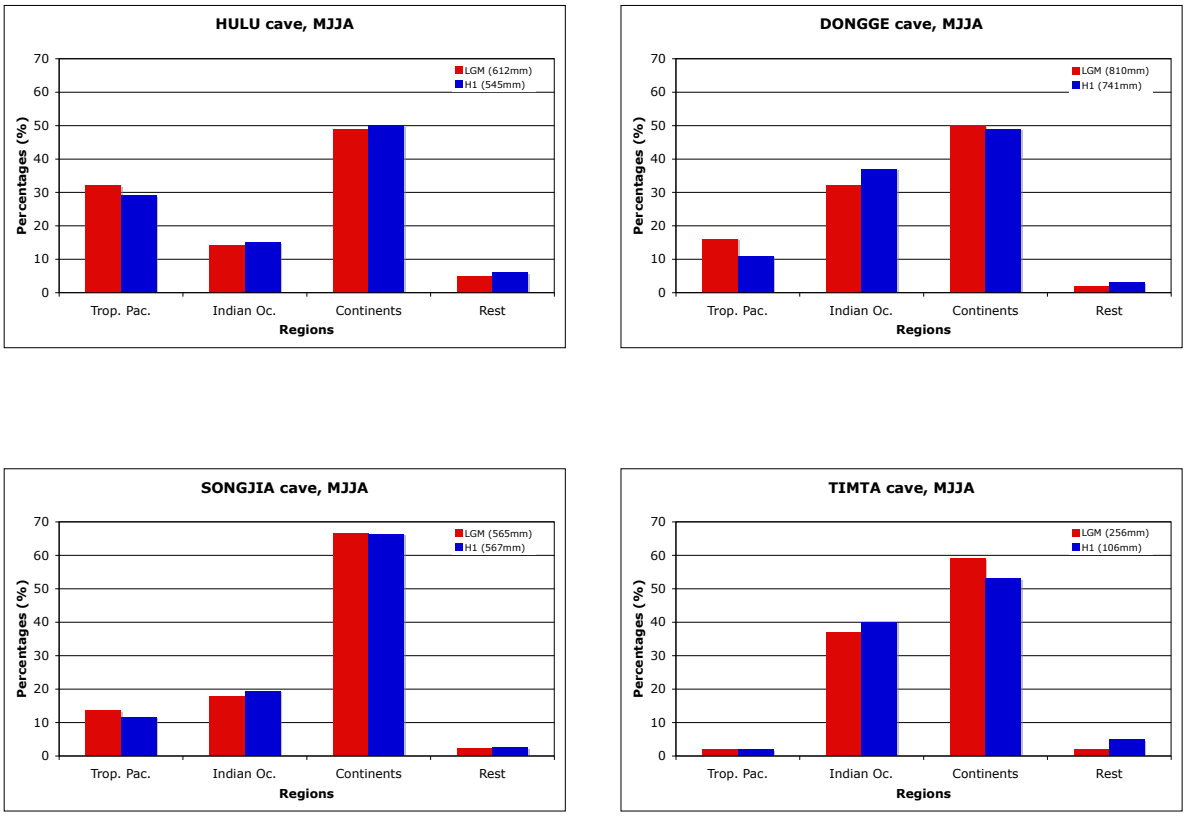

Fig. S5: H1 (blue) and LGM (red) percentage of MJJA precipitation originating from each tagged region for the cave sites shown in Fig. S1. The amount of precipitation falling in MJJA for the two climate simulations is indicated in parentheses.

1. *H1onlyATL*: CAM3 forced with LGM boundary conditions, except for the SST and sea ice in the North Atlantic that are prescribed from the H1 experiment.

2. *H1exceptIND*: CAM3 forced with H1 boundary conditions, except for the SST in the Indian Ocean that is prescribed from LGM experiment.

3. *H1onlyIND*: CAM3 forced with LGM boundary conditions, except for SST in the Indian Ocean that is prescribed from the H1 experiment.

Figure S6 shows the annual average temperature change (compared to the LGM experiment) that results from these three experiments as well as from the full H1 experiment. The abrupt cooling in the North Atlantic alone (H1onlyATL) accounts for almost all of the cooling over the Northern Hemisphere seen in the H1 experiment. Note that in the H1onlyIND, even though the temperature at the site of the Chinese caves is actually slightly higher than that in the LGM simulation, the $\delta^{18}O_p$ is similar to the H1 experiment (Fig. 3 in the main manuscript). The changes in the $\delta^{18}O$ and $\delta^{18}O_p$ from the three experiments are discussed in the text.

Crucial SST changes and key processes responsible for changes in $\delta^{18}O_p$

Here we present a brief discussion that illuminates the regional changes in climate that are predominantly responsible for the $\delta^{18}O_p$ changes seen in the H1 experiment (compared to the LGM). First, in figure S7 top row we show a breakdown of the various sources that contribute to the changes in $\delta^{18}O_p$ by tracking the water vapor and its isotopic composition from three key source regions: Tropical Pacific Ocean (left), Indian Ocean (center) and continental regions (right). The first row of panels shows that the total change in $\delta^{18}O_p$ (H1 minus LGM) over northern India is due to changes in the $\delta^{18}O$ of precipitation (and reduced summer precipitation) originated in the Indian Ocean basin and from recycling.

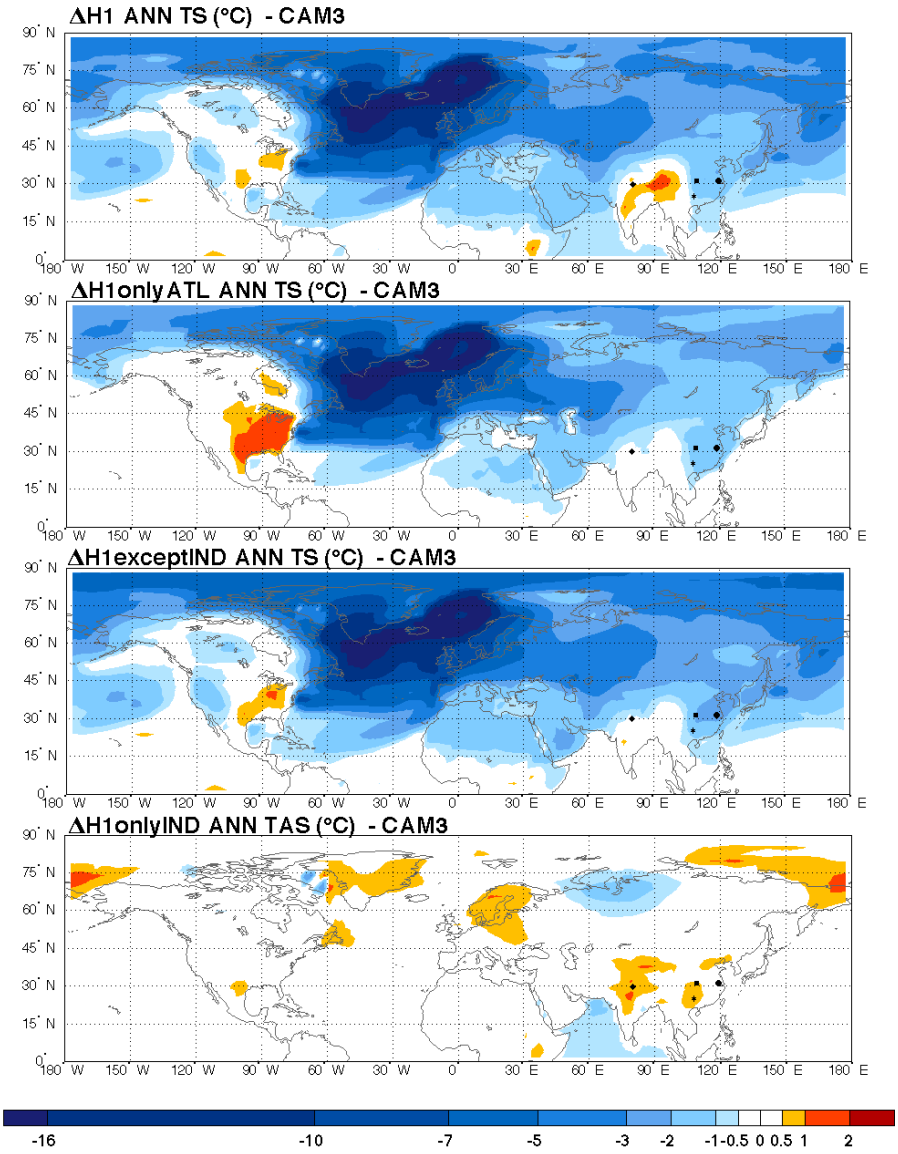

Fig. S6: Change in the annual averaged surface temperature for the experiments using partial SST changes. From top to bottom: H1 minus LGM, H1onlyATL minus LGM, H1exceptIND minus LGM, and H1onlyIND minus LGM. Markers indicate the location of the following caves: Hulu (circle), Songjia (square), Dongge (star), Timta (diamond).

The final row shows the changes in $\delta^{18}O_p$ due solely to the changes in SST in the Indian Ocean. The similarity between the top row and the bottom row is striking and illustrates that the lion's share of the $\delta^{18}O_p$ changes seen in the H1 experiment stem solely from changes in the

Indian Ocean SST (which, of course, is directly due to the changes in sea ice and SST in the North Atlantic; Fig. S6).

The second row of panels shows that changes in SST and sea ice in the North Atlantic alone have no impact on the δ^{18}O of precipitation over all Asia. Results from the simulation that incorporates all of the SST and sea ice changes from the H1 experiment *except* the Indian Ocean SST changes are shown in the third row. Here we see that changes in the boundary conditions (most likely in the tropical Pacific SST) contribute to an increase in $\delta^{18}O_p$ over China which are in part canceled by a reduction in the local continental source.

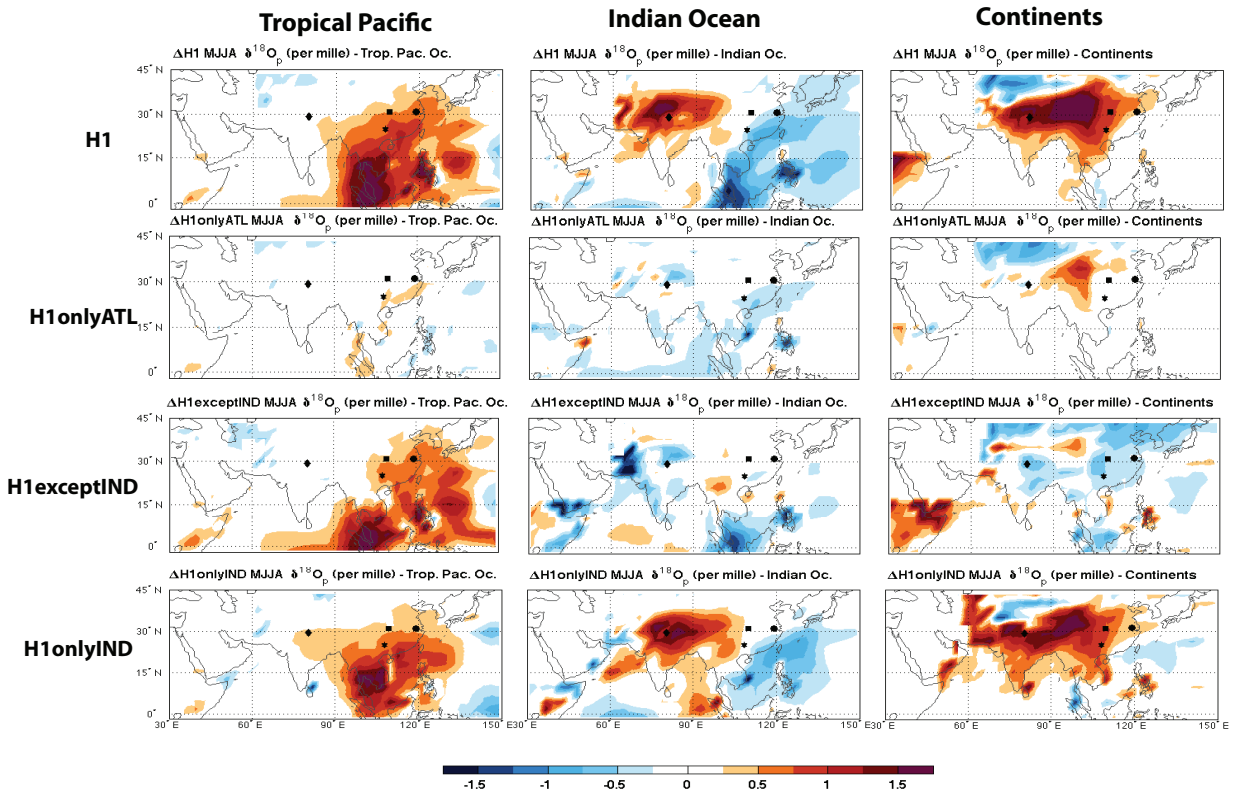

Fig. S7: Regional contributions to the change in the MJJA precipitation weighted δ^{18}O for the various pairs of experiments: H1 - LGM (top), H1onlyATL - LGM (upper middle), H1exceptIND - LGM (lower middle), and H1onlyIND -LGM (bottom). Shown from left to right for each pair of experiments is the contribution to the MJJA precipitation weighted δ^{18}O from the Tropical Pacific Ocean (left), Indian Ocean (middle) and the continents (right) . Markers indicate the location of the following caves: Hulu (circle), Songjia (square), Dongge (star), Timta (diamond).

Sea surface temperature in the Indian Ocean and the Indian Monsoon

The changes in the Indian Ocean SST are crucial for explaining the $\delta^{18}O_p$ changes during abrupt climate changes. Figure S8 shows the bi-monthly averaged changes in the Indian Ocean SST simulated in the H1 with respect to LGM experiment in the coupled CCSM. The cooling of

the Indian Ocean (more pronounced in winter/early spring) leads to a delay in the onset of the Indian summer monsoon and a decrease in precipitation over the Indian Ocean and subcontinent in summer.

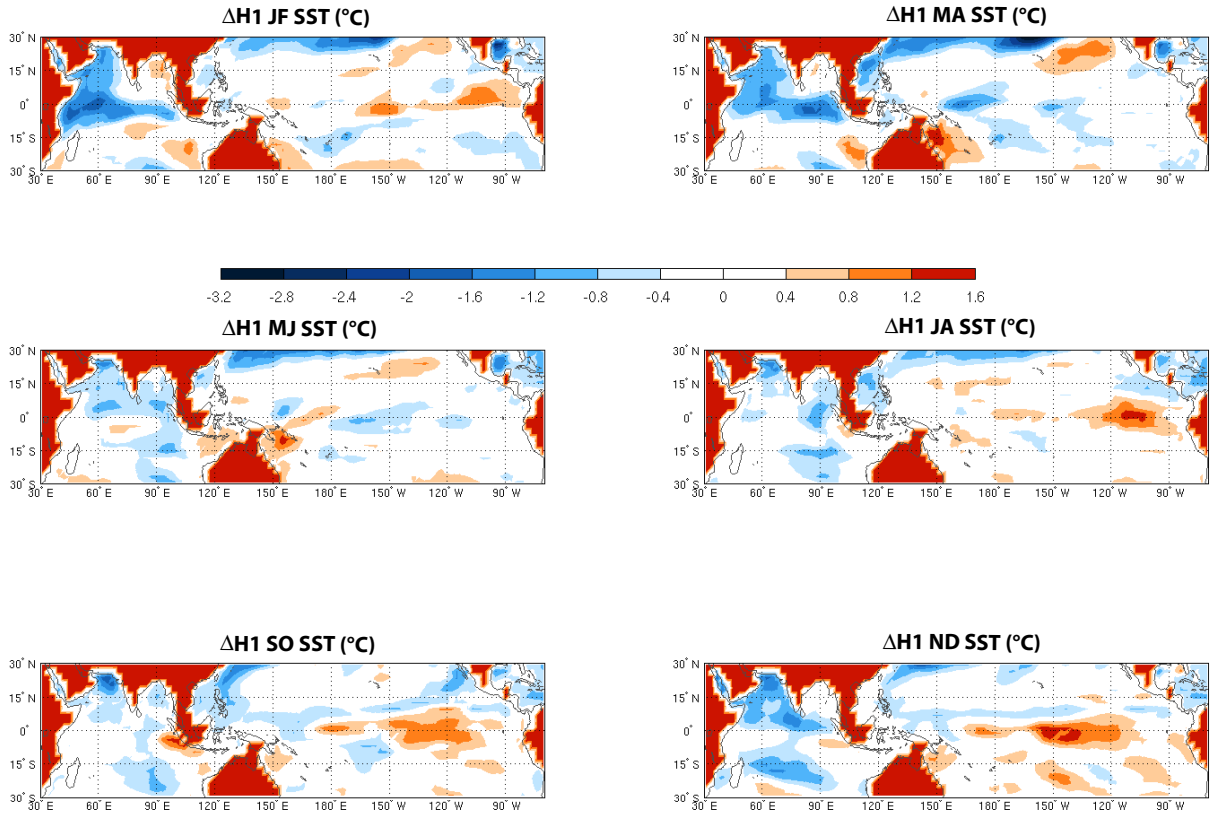

Fig. S8: Change in SST in the H1 compared to the LGM experiment, presented bimonthly.

We used the South Asian Monsoon (SAM) index from Goswami et al. (*9*) as a dynamical measure of the strength of the Indian monsoon. The SAM is defined as the vertical shear (850 hPa - 200 hPa) of the meridional component of the wind (V) and measures the overtuning over south Asia and the Indian Ocean associated with the local Hadley cell (10°-30°N, 70°-110°E). The SAM index for each experiment is shown in figure S9. Note that in the H1 experiment the monsoon index is less than half that in the LGM experiment and the summer monsoon season starts later and ends earlier in the H1 experiment compared to the LGM experiment. Hence, the

duration of the monsoon (as defined by the time the SAM index exceeds zero) is about three weeks shorter in the H1 experiment than in the LGM experiment (Fig. S9).

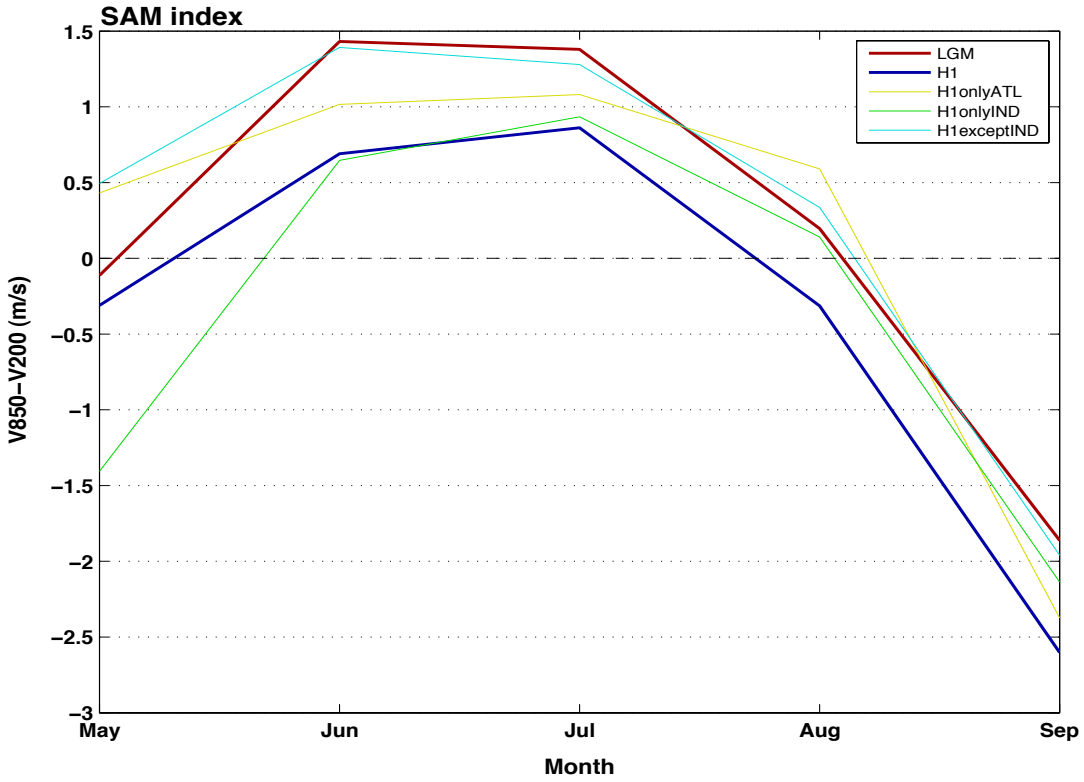

Fig. S9: May to September South-Asia Monsoon index for LGM, H1, H1onlyATL, H1onlyIND and H1exceptIND experiments.

Response to freshwater dumps into the North Atlantic during modern day versus LGM

We note Lewis et al. (*10*) have performed a study to examine the impact of a sudden freshwater pulse into the North Atlantic on the climate and isotopic composition of precipitation. The fresh water pulse in their study is applied to a world that has a modern day distribution of land ice and Holocene values for carbon dioxide and other greenhouse gases. We also examine the changes in the climate and isotopic composition of precipitation to a large freshwater dump in

the North Atlantic, but we do so using a geometry and basic state that closely represents the last glacial period. The most notable differences between their experiments and ours are in the extent and size of the ice sheets and the concentration of greenhouse gases. Dynamical theory and scores of GCM calculations demonstrate there are large differences in the response of the atmosphere to forcing with ice sheets present compared to without ice sheets (i.e., in modern day geometry) (*1, 11*) . Furthermore, hosing experiments carried out with the same climate model (CCSM3) show that the change in precipitation over southern and eastern Asia due to hosing during the Holocene is very different from that during the last glacial period (Fig. S10). Lewis et al. (*10*) find enhanced sea ice during the Holocene causes a slightly wetter southern (slightly drier northern) China, but little or no impact on the $\delta^{18}\mathrm{O}_p$ over Eastern China (which is consistent with what is to be expected from the analyses of the instrumental records of modern day $\delta^{18}\mathrm{O}_p$ over China (*12, 13*)). Not surprisingly, we find the same result using CCSM3 for the Holocene case (compare Fig. S10 left with Fig. 4 in Lewis et al. (*10*)). The enhanced sea ice extent that results from a freshwater dump in a glacial period features even smaller changes in precipitation over China, but importantly it causes a much greater reduction in the precipitation over the Indian Ocean. The freshwater dump in the glacial climate results in a much shorter and weakened Indian summer monsoon (ISM) than in the Holocene climate, which is solely responsible for the enhancement in the $\delta^{18}\mathrm{O}$ of precipitation over China that is recorded in the speleothems. The weaker ISM in the LGM compare to the Holocene is presumably due to the stronger glacial winds that distribute the cooling in the North Atlantic over a greater spatial extent.

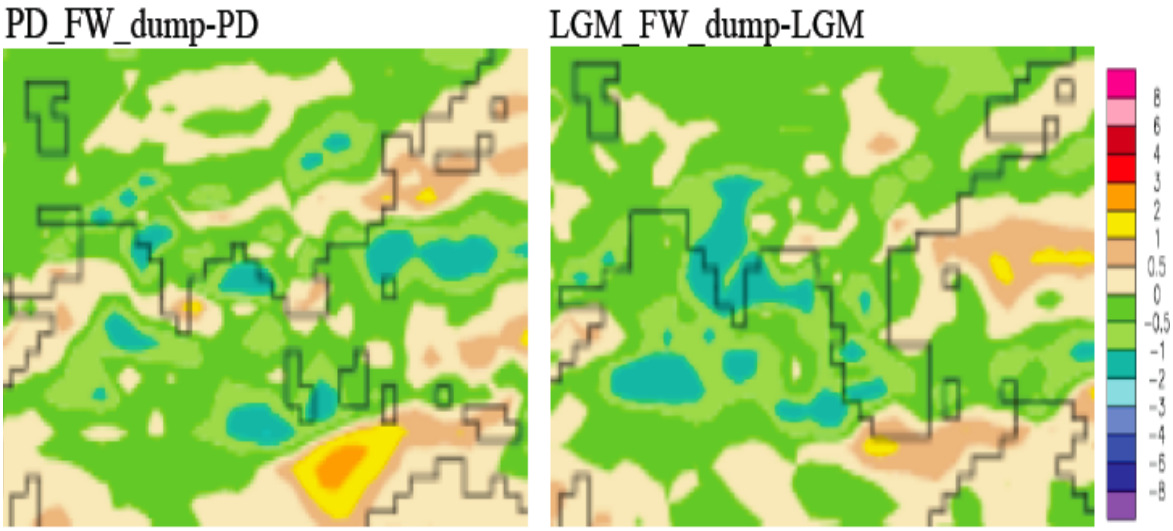

Fig. S10: Change in the precipitation over Southern and Eastern Asia (the area in the box in Fig. S4) when freshwater is suddenly applied to a control climate integration of the modern climate (left) and LGM climate (right). Units are mm/day.

Biases in the atmospheric model

The atmosphere model (CAM3) is able to capture the major features of the East Asian Monsoon (EASM) circulation system, including the large scale circulation and the gross aspects of precipitation. Considerable discrepancies exist in the the precise location of precipitation on smaller (sub basin) scales (*14*) but these deficiencies are not of consequence for the issues we examine in this paper. Our results show that the speleothems across China are recording the

changes in the isotopic composition of the vapor that is advected in from the Indian Ocean, and that the isotopic changes come about because of gross changes in the intensity and duration of the Indian monsoon. Although the exact spatial distribution of the simulated precipitation may be sensitive to model physics (e.g., the choice of convective scheme), the overall intensity and duration of the Indian monsoon is determined by basic thermodynamical constraints (*15–17*) that tie precipitation to the surface moist static energy which, in turn, is strongly determine by SST in the northern Indian Ocean. Hence, downwind of the monsoon region (e.g., over eastern China) the isotopic signature of the monsoon strength is insensitive to details in the spatial distribution of precipitation and is robust to any biases in the detailed distribution of precipitation (e.g., the precise distribution of precipitation on small scales). Indeed, our results help explain why the speleothems spread across China are so highly correlated temporally and why they so robustly record abrupt climate changes during the last glacial period: it is because the caves are recording changes in the isotopic composition of the vapor which is set by the spatially integrated changes in the Indian monsoon intensity and distributed eastward by winds to create a ubiquitous continental scale signature in the caves across China. It is precisely for this reason that the Chinese speleothems are in fact a robust proxy of the Indian monsoon.

References

1. Bitz, C. M., Chiang, J. C. H., Cheng, W. & Barsugli, J. J. Rates of thermohaline recovery from freshwater pulses in modern, Last Glacial Maximum, and greenhouse warming climates. *Geophys. Res. Lett.* **34**, L07708 (2007).

2. Cheng, W., Bitz, C. M. & Chiang, J. C. H. *Adjustment of the global climate to an abrupt slowdown of the Atlantic meridional overturning circulation* (AGU monograph, 2007). Pp. 295-313.

3. Otto-Bliesner, B. L. *et al.* Last Glacial Maximum and Holocene climate in CCSM3. *J. Clim.* **19**, 2526–2544 (2006).

4. Braconnot, P. *et al.* Results of PMIP2 coupled simulations of the Mid-Holocene and Last Glacial Maximum - Part 1: experiments and large-scale features. *Clim. Past* **3**, 261–277 (2007).

5. Hemming, S. R. Heinrich events: Massive late Pleistocene detritus layers of the North Atlantic and their global climate imprint. *Reviews of Geophysics* **42**, RG1005 (2004).

6. Collins, W. D. *et al.* The formulation and atmospheric simulation of the Community Atmosphere Model version 3 (CAM3). *J. Clim.* **19**, 2144–2161 (2006).

7. Sturm, C., Zhang, Q. & Noone, D. An introduction to stable water isotopes in climate models: benefits of forward proxy modelling for paleoclimatology. *Clim. Past* **6**, 115–129 (2010).

8. Gill, A. E. Some simple solutions for heat-induced tropical circulation. *Q. J. R. Meteorol. Soc.* **106**, 447–462 (1980).

9. Goswami, B. N., Krishnamurthy, V. & Annamalai, H. A broad-scale circulation index for the interannual variability of the Indian summer monsoon. *Q. J. R. Meteorol. Soc.* **125**, 611–633 (1999).

10. Lewis, S. C., LeGrande, A. N., Kelley, M. & Schmidt, G. A. Water vapour source impacts on oxygen isotope variability in tropical precipitation. *Clim. Past* **6**, 325–343 (2010).

11. Swingedouw, D. *et al.* Impact of freshwater release in the north atlantic under different climate conditions in an oagcm. *J. Clim.* **22**, 6377–6403 (2009).

12. Johnson, K. R., Ingram, B. L., Sharp, W. D. & Zhang, P. Z. East Asian summer monsoon variability during Marine Isotope Stage 5 based on speleothem delta O-18 records from Wanxiang Cave, central China. *Palaeography Palaeoclimatology Paleoecology* **236** , 5–19 (2006).

13. Dayem, K. E., Molnar, P., Battisti, D. S. & Roe, G. H. Lessons learned from oxygen isotopes in modern precipitation applied to interpretation of speleothem records of paleoclimate from eastern Asia. *Earth and Planetary Science Letters* **295**, 219–230 (2010).

14. Chen, H., Zhou, T., Neale, R. B., Wu, X. & Zhang, G. J. Performance of the New NCAR CAM3.5 in East Asian Summer Monsoon Simulations: Sensitivity to Modifications of the Convection Scheme. *J. Clim.* **23**, 3657–3675 (2010).

15. Emanuel, K. A., Neelin, J. D. & Bretherton, C. S. On large-scale circulations in convecting atmospheres. *Q. J. R. Meteorol. Soc.* **120**, 1111–1143 (1994).

16. Emanuel, K. A. *Quasi-equilibrium dynamics of the tropical atmosphere* (Princeton Univ. Press, 2007). Pp. 186-218.

17. Neelin, J. D. *Moist dynamics of tropical convection zones in monsoons, teleconnections, and global warming* (Princeton Univ. Press, 2007). Pp. 186-218.